

1
2
3
4 **A Piecewise-Linearized Cell Transmission Model and Parameter Calibration Methodology**
5

6 Laura Muñoz, Xiaotian Sun, Roberto Horowitz, and Luis Alvarez
7

8 Laura Muñoz *

9 Department of Mechanical Engineering
10 University of California, Berkeley, CA 94720
11 Phone: (510) 642-5109, Fax: (510) 643-5599
12 lmunoz@me.berkeley.edu
13

14 Xiaotian Sun

15 Department of Mechanical Engineering
16 University of California, Berkeley, CA 94720
17 Phone: (510) 643-8903, Fax: (510) 643-5599
18 sunx@me.berkeley.edu
19

20 Roberto Horowitz

21 Department of Mechanical Engineering
22 University of California, Berkeley, CA 94720
23 Phone: (510) 642-4675, Fax: (510) 643-5599
24 horowitz@me.berkeley.edu
25

26 Luis Alvarez

27 Instituto de Ingeniería
28 Universidad Nacional Autónoma de México, México D.F., 04510
29 Phone: +52(5) 62 281 29, Fax: +52(5) 62 281 30
30 alvar@pumas.iingen.unam.mx
31

32 * Corresponding Author
33
34

35 Submission date: November 21, 2005
36

37 Word count: 9788 (7788 in text, plus 2000 from 6 figures and 2 tables at 250 words each)
38
39
40
41
42
43
44
45
46
47
48
49
50
51
52

ABSTRACT

This paper concerns the development of macroscopic freeway traffic models and parameter calibration methodologies that are computationally efficient and suitable for use in real-time traffic monitoring and control applications. Toward the fulfillment of these objectives, a macroscopic traffic model, the Switching-Mode Model (SMM), is presented, which is a piecewise linearized version of Daganzo's Cell Transmission Model (CTM). The observability and controllability properties of the SMM modes are reviewed, since these properties are of fundamental importance in the design of traffic estimators and on-ramp metering controllers.

A semi-automated method has been developed for calibrating the CTM and SMM parameters. In this method, a least-squares data fitting approach is applied to loop detector data to determine free-flow speeds, congestion-wave speeds, and jam densities for specified subsections of a freeway. Bottleneck capacities are estimated from measured mainline and on-ramp flows. The calibration method was tested using loop detector data from an approximately 14-mile (23 km) section of Interstate 210 West (I-210W) in southern California. Traffic data sources were the Performance Measurement System (PeMS), and a set of manually-counted ramp volumes provided by Caltrans District 7. Parameters were first calibrated for a short (2 mi (3 km)) subsection of I-210W and tested on both the SMM and CTM, which were shown to perform similarly to one another. The calibration method was then extended to the full 14-mi section, and the parameters were tested with the CTM. The CTM was able to reproduce observed bottleneck locations and the general behavior of traffic congestion, yielding approximately 2% average error in predicted total travel time.

INTRODUCTION

Accurate freeway traffic models are extremely valuable tools for the design and evaluation of traffic monitoring and management strategies. An example of the latter application (as in (1, 2)) is the use of calibrated macroscopic and microscopic traffic models to predict the effects of different on-ramp metering algorithms, prior to performing field tests. However, the calibration of traffic models, particularly those that are microscopic, is often laborious and time-consuming. As discussed in (3), the topics of traffic model calibration and validation remain an active area of research, and there is a need for a standardized set of calibration guidelines. To help fulfill the goal of providing an accurate, computationally efficient and easy-to-calibrate model for the development and analysis of on-ramp metering algorithms, a piecewise-linearized version of Daganzo's macroscopic Cell Transmission Model (CTM) (4, 5), called the Switching-Mode Model (SMM), has been developed (6), and will be discussed in this paper. Its linear structure lends the advantage of simplifying control analysis, design, and data-estimation methods. The CTM, which will be described briefly, has many favorable features, particularly its simplicity, ease of calibration, and its ability to reproduce important traffic phenomena such as shock wave propagation. These properties are also inherited by the SMM. Both the CTM and SMM have been shown to perform well in describing traffic behavior when tested with data from a 2-mile (3 km) portion of Interstate 210 Westbound (I-210W) in southern California (6, 7). Furthermore, the observability and controllability properties of the SMM, which are of fundamental importance in the design of traffic data estimators and freeway on-ramp control systems, can be derived using standard linear systems techniques, as discussed later in this paper. In order to facilitate the calibration of the CTM and SMM, a semi-automated calibration methodology for estimating their common parameters has been developed (7, 8), and a preliminary comparison has been made to the data imputation methods reported in (9).

This research has focused on a segment of I-210W, shown in Fig. 1, which typically endures heavy congestion during the weekday morning commute period. It is approximately 14 miles (23 km) long, from Vernon (postmile 39.159) to Fair Oaks (postmile 25.4), with 20 metered on-ramps, one un-metered freeway-to-freeway entrance, and 18 off-ramps.

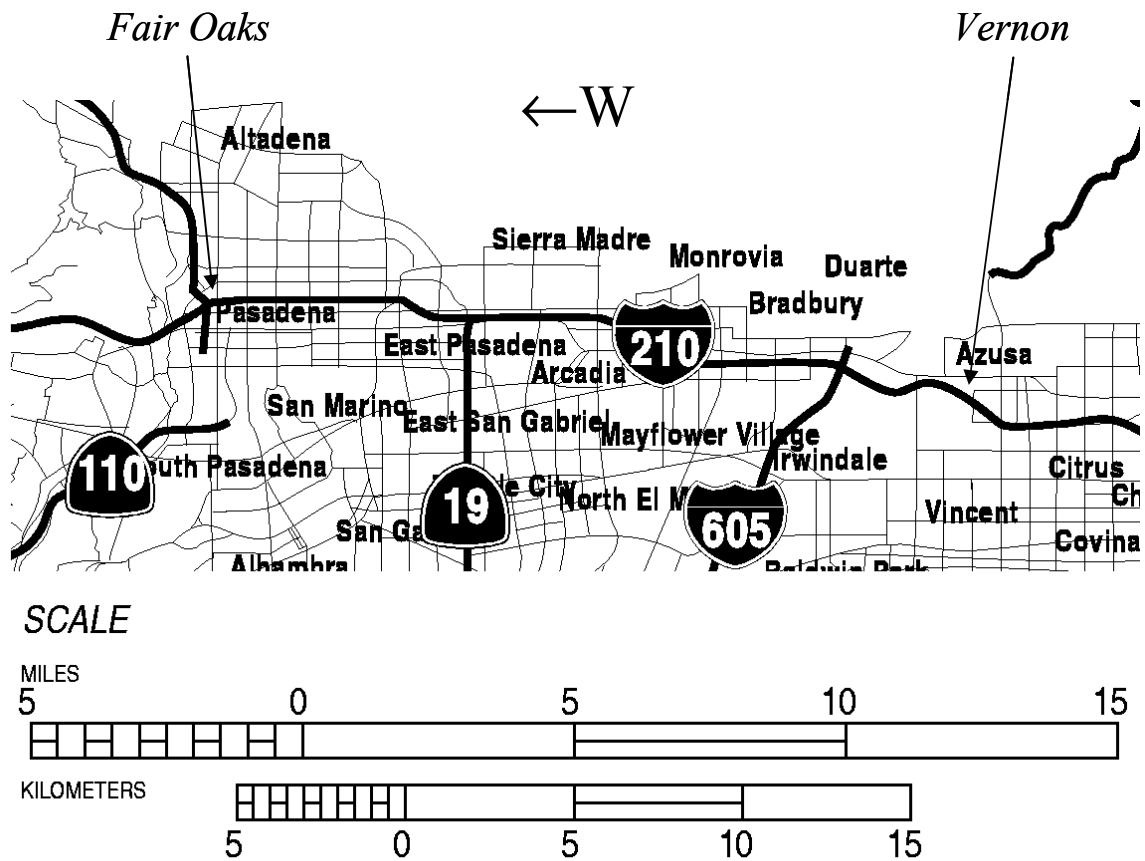


FIGURE 1 I-210 test segment. Extracted from Caltrans District 7 Base Map.fh10, 3/5/03, a public domain map.

CELL TRANSMISSION MODEL

The CTM was selected for this research due to its analytical simplicity and ability to reproduce important traffic behavioral phenomena, such as the backward propagation of congestion waves. The CTM has previously been validated for a single freeway link, with no on-ramps or off-ramps, using data from I-880 in California (10). A more complete description of the model can be found in (4, 5, 11), but the main equations will be reviewed in this section.

In the CTM, a freeway is partitioned into a series of cells. A 4-cell example is shown in Fig. 2.

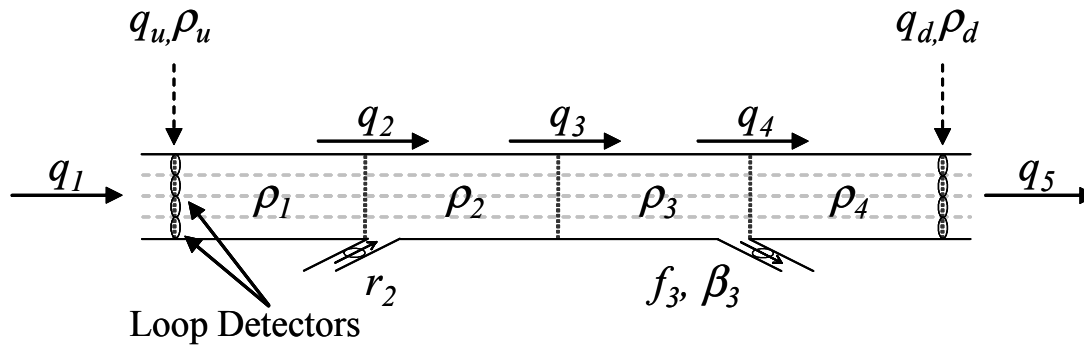


FIGURE 2 Freeway segment divided into 4 cells.

Here, $\rho_i(k)$ is the density, in vehicles per unit length of freeway, in cell i at time kT_s , where k is the time index and T_s is the discrete time interval. The density evolves according to conservation of vehicles:

$$\rho_i(k + 1) = \rho_i(k) + \frac{T_s}{l_i}(q_{i,in}(k) - q_{i,out}(k)) \quad (1)$$

where $q_{i,in}(k)$ and $q_{i,out}(k)$ are, respectively, the total flows, in vehicles per unit time, entering and leaving cell i during the k^{th} time interval, $T_s [k, k+1)$, including flows along the mainline and the on- and off-ramps, and l_i is the length of cell i .

The model parameters include v , w , Q_M , and ρ_J , which are depicted in the trapezoidal fundamental diagram of Fig. 3. The parameters can be uniform over all cells or allowed to vary from cell to cell.

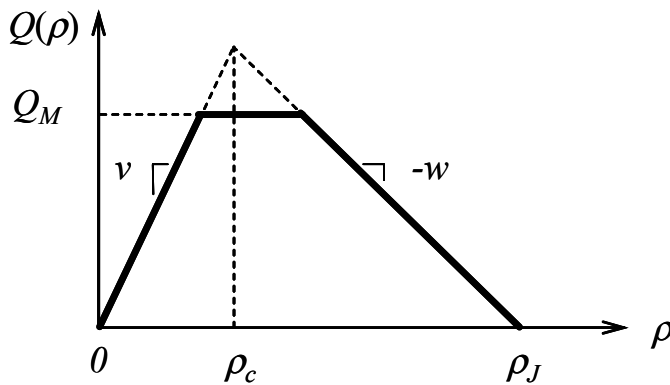


FIGURE 3 Trapezoidal fundamental diagram.

The parameters are defined as:

- v ... free-flow speed (miles per hour (mph) or km per hour (kph))
- w ... backward congestion wave speed (mph or kph)
- Q_M ... maximum allowable flow (veh/hr, i.e., vph)
- ρ_J ... jam density (veh/mi (vpm) or veh/km (vpk), or per lane (vpmpl, vpkpl))
- ρ_c ... critical density (vpm, vpk, vpmpl or vpkpl)

A trapezoidal fundamental diagram was chosen for the CTM, since this type of diagram is a standard formulation for the model (5), and lends itself easily to the piecewise linearization described in this paper. The simulation results presented in this paper show that the CTM, with a trapezoidal diagram, appears sufficient to allow the model to capture observed traffic behavior. However, a trapezoidal diagram is not mandatory; it is possible to implement the CTM with other diagram shapes, as discussed in (11).

Three different types of intercellular connection are allowed: simple connection, merge, and diverge. In a simple connection, two cells are connected to one another without any intervening on-ramps or off-ramps (e.g., cells 2 and 3 in Fig. 2). Let $i-1$ be the upstream cell and i be the downstream cell in the pair. As described in (5), $q_i(k)$, the flow entering cell i from the mainline, is determined by taking the minimum of two quantities:

$$q_i(k) = \min(S_{i-1}(k), R_i(k)), \quad (2)$$

$$S_{i-1}(k) = \min(v_{i-1}\rho_{i-1}(k), Q_{M,i-1}), \quad (3)$$

$$R_i(k) = \min(Q_{M,i}, w_i(\rho_{J,i} - \rho_i(k))), \quad (4)$$

where $S_{i-1}(k)$ is the maximum flow that can be *supplied* by cell $i-1$ under free-flow conditions, over the k^{th} time interval, and $R_i(k)$ is the maximum flow that can be *received* by cell i under congested conditions, over the same time interval.

In the work presented here, simplified versions of the CTM merge and diverge laws of (5) were used. These simplified laws are appropriate for calibration tests for freeways that are free of off-ramp bottlenecks; a complete statement of these laws can be found in (7). A merge and diverge are shown within the context of a freeway segment in Fig. 2, where q_2 and r_2 are the flows merging into cell 2, and q_4 and f_3 are the flows diverging from cell 3. The diverging flows are defined as $q_4(k) = (1-\beta_3(k))q_{3, out}(k)$, and $f_3(k) = \beta_3(k)q_{3, out}(k)$, where $\beta_3(k)$ is the *split ratio* for the diverge junction, i.e., the fraction of vehicles leaving cell 3 which exits through the off-ramp during the k^{th} time interval. It is assumed here that the split ratios can be determined externally to the model as functions of time. The version of the CTM used in this work consists of flow conservation, Eq. (1), for each cell, along with the flow specification (e.g., Eq. (2)) for each intercellular connection. The state variable is $\boldsymbol{\rho} = [\rho_1 \dots \rho_N]^T$ for a freeway partitioned into N cells, and the model inputs are the measured flows entering the freeway at the upstream mainline boundary and at each on-ramp merge location.

For reference, *congestion* refers to the traffic condition that occurs when vehicle density is high, and drivers proceed at reduced speeds in order to avoid collisions. *Free-flow* is the opposite condition, where vehicle density is low, and drivers travel at high speeds. The left part of the fundamental diagram of Fig. 3, where $Q(\rho) = v\rho$, is an approximation of the typical behavior of free-flow traffic, whereas the right side ($Q(\rho) = w(\rho_J - \rho)$) is associated with congested traffic. For the case in which the fundamental diagram is triangular, instead of trapezoidal, the *congestion status* of cell i is determined by comparing the cell density with the critical density: if $\rho_i < \rho_{c,i}$, the cell has free-flow status, otherwise $\rho_i \geq \rho_{c,i}$ and the cell has congested status.

SWITCHING-MODE MODEL

In order to gain additional insight into freeway traffic behavior, and to simplify the control analysis, control design, and data-estimation design methods, a piecewise-linearized version of the CTM, called the switching-mode model (SMM), has been designed (6, 7). Since the SMM is composed of several linear models, straightforward linear techniques for model analysis and control design can be applied to the individual linear subsystems.

The SMM can be extracted from the CTM by writing each inter-cellular flow as either an explicit function of cell density, or as a constant. In the case of a segment without merges or diverges, each q_i would be replaced with $v\rho_{i-1}(k)$, $w(\rho_j - \rho_i(k))$, or Q_M . This explicit density dependence is achieved by supplying a set of logical rules that determine the congestion status of each cell, at every time step, based on measurements at the segment boundaries.

For simplicity, it is assumed that a freeway section can only be in one of five modes: (1) “free-flow—free-flow” (FF), in which all cells in the section have free-flow status, (2) “congestion—congestion” (CC), in which all cells in the section have congested status, (3) “congestion—free-flow” (CF), in which the upstream part of the section is congested and the downstream part has free-flow status, (4) “free-flow—congestion 1” (FC1), in which the upstream part of the section has free-flow status, the downstream part has congested status, and the boundary (i.e., wave front) separating the two regions is moving downstream, and (5) “free-flow—congestion 2” (FC2), in which the upstream part of the section has free-flow status, the downstream part has congested status, and the wave front separating the two regions is moving upstream. This set of modes covers the possible congestion patterns within a section that has, at most, one status transition, referred to here as a wave front. The single-wave front assumption is an approximation that is expected to be acceptable for short freeway sections. To more accurately deal with longer sections, the SMM can be modified to allow multiple wave fronts within a section.

Note that the SMM does not fully replicate the CTM merge and diverge laws described in (5). While the on-ramp entering ($r(k)$) and off-ramp exiting (e.g., $\beta(k) v_i \rho_i$) flows are represented in the SMM, the ramps are not modeled by cells; hence, the traffic densities on the ramps are not represented.

These simplifications are considered reasonable when (1) the SMM is being used in a calibration or validation study; in this case, $r(k)$ is set equal to the measured flow merging onto the freeway from the associated on-ramp (this quantity is typically available from field measurements), and (2) the selected freeway segment contains no “off-ramp bottlenecks”, or more generally, there are no situations where congestion originates on an off-ramp due to insufficient capacity on the off-ramp. Review of the traffic data from the I-210 segment, discussed in part in (7, 12), indicates that the segment does not appear to exhibit any off-ramp bottlenecks or off-ramp congestion, hence, the SMM off-ramp flow representation is reasonable. If the SMM is used as a basis for designing ramp-metering controllers, as in (1), it is advisable to additionally consider an on-ramp queuing model (see (1) for more detail).

Consider the freeway segment in Fig. 2, which is divided into 4 cells. The measured aggregate flows and densities at the upstream and downstream mainline detectors are denoted by q_u, ρ_u , and q_d, ρ_d . All five modes of the SMM can be summarized as follows:

$$\boldsymbol{\rho}(k+1) = A_s \boldsymbol{\rho}(k) + B_s \mathbf{u}(k) + B_{J,s} \boldsymbol{\rho}_J + B_{Q,s} \mathbf{q}_M, \quad (5)$$

where $s = 1, 2, 3, 4, 5$ indicates the mode (1: FF, 2: CC, 3: CF, 4: FC1, 5: FC2), $\boldsymbol{\rho} = [\rho_1 \dots \rho_4]^T$ is the state, and $\mathbf{u} = [q_u \ r_2 \ \rho_d]^T$ are the flow and density inputs. r_2 is the measured on-ramp flow entering the section, subscripted according to its cell of entry. $\boldsymbol{\rho}_J = [\rho_{J,1} \ \rho_{J,2} \ \rho_{J,3} \ \rho_{J,4} \ \rho_{J,5}]^T$ is the vector of jam densities, and $\mathbf{q}_M = [Q_{M,1} \ Q_{M,2} \ Q_{M,3} \ Q_{M,4}]^T$ is the vector of maximum flow rates.

In free-flow mode, the flow across each cell boundary is dictated by *upstream* conditions. Each cell releases traffic at the free-flow rate, i.e., the total flow exiting cell i is given by $v_i \rho_i$. The state equation is:

$$\begin{aligned} \begin{bmatrix} \rho_1 \\ \rho_2 \\ \rho_3 \\ \rho_4 \end{bmatrix} (k+1) &= \begin{bmatrix} 1 - \frac{v_1 T_s}{l_1} & 0 & 0 & 0 \\ \frac{v_1 T_s}{l_2} & 1 - \frac{v_2 T_s}{l_2} & 0 & 0 \\ 0 & \frac{v_2 T_s}{l_3} & 1 - \frac{v_3 T_s}{l_3} & 0 \\ 0 & 0 & (1 - \beta_3(k)) \frac{v_3 T_s}{l_4} & 1 - \frac{v_4 T_s}{l_4} \end{bmatrix} \begin{bmatrix} \rho_1 \\ \rho_2 \\ \rho_3 \\ \rho_4 \end{bmatrix} (k) \\ &+ \begin{bmatrix} \frac{T_s}{l_1} & 0 & 0 \\ 0 & \frac{T_s}{l_2} & 0 \\ 0 & 0 & 0 \\ 0 & 0 & 0 \end{bmatrix} \begin{bmatrix} q_u \\ r_2 \\ \rho_d \end{bmatrix} (k) \\ &= A_1(k) \boldsymbol{\rho}(k) + B_1 \mathbf{u}(k). \end{aligned} \quad (6)$$

In CC mode, the flow across each cell boundary is dictated by *downstream* conditions, i.e., the total flow entering cell i is given by $w_i(\rho_{J,i} - \rho_i)$. The flow released by cell 4 is determined by the downstream density ρ_d . The state equation is:

$$\begin{aligned} \begin{bmatrix} \rho_1 \\ \rho_2 \\ \rho_3 \\ \rho_4 \end{bmatrix} (k+1) &= \begin{bmatrix} 1 - \frac{w_1 T_s}{l_1} & \frac{w_2 T_s}{l_1} & 0 & 0 \\ 0 & 1 - \frac{w_2 T_s}{l_2} & \frac{w_3 T_s}{l_2} & 0 \\ 0 & 0 & 1 - \frac{w_3 T_s}{l_3} & \frac{1}{1 - \beta_3(k)} \frac{w_4 T_s}{l_3} \\ 0 & 0 & 0 & 1 - \frac{w_4 T_s}{l_4} \end{bmatrix} \begin{bmatrix} \rho_1 \\ \rho_2 \\ \rho_3 \\ \rho_4 \end{bmatrix} (k) \\ &+ \begin{bmatrix} 0 & \frac{T_s}{l_1} & 0 \\ 0 & 0 & 0 \\ 0 & 0 & 0 \\ 0 & 0 & \frac{w_5 T_s}{l_4} \end{bmatrix} \begin{bmatrix} q_u \\ r_2 \\ \rho_d \end{bmatrix} (k) + \begin{bmatrix} \frac{w_1 T_s}{l_1} & -\frac{w_2 T_s}{l_1} & 0 & 0 \\ 0 & \frac{w_2 T_s}{l_2} & -\frac{w_3 T_s}{l_2} & 0 \\ 0 & 0 & \frac{w_3 T_s}{l_3} & -\frac{1}{1 - \beta_3(k)} \frac{w_4 T_s}{l_3} \\ 0 & 0 & 0 & \frac{w_4 T_s}{l_4} \end{bmatrix} \begin{bmatrix} \rho_{J,1} \\ \rho_{J,2} \\ \rho_{J,3} \\ \rho_{J,4} \\ \rho_{J,5} \end{bmatrix} \\ &= A_2(k) \boldsymbol{\rho}(k) + B_2 \mathbf{u}(k) + B_{J,2}(k) \boldsymbol{\rho}_J. \end{aligned} \quad (7)$$

In CF mode, there exists one congestion-to-free-flow transition inside the section. One assumption of the SMM is that the wave front will always lie on a cell boundary. Cells upstream of the wave front accept vehicles at the congested flow rate, while cells downstream of the wave

front release vehicles at the free-flow rate. The wave front acts as a bottleneck, expelling vehicles at maximum allowed rate Q_M , and decoupling the region upstream of the wave front from the downstream region. For the case where the wave front is located in between cells 2 and 3, the state equation is:

$$\begin{aligned}
 \begin{bmatrix} \rho_1 \\ \rho_2 \\ \rho_3 \\ \rho_4 \end{bmatrix} (k+1) &= \begin{bmatrix} 1 - \frac{w_1 T_s}{l_1} & \frac{w_2 T_s}{l_1} & 0 & 0 \\ 0 & 1 - \frac{w_2 T_s}{l_2} & 0 & 0 \\ 0 & 0 & 1 - \frac{v_3 T_s}{l_3} & 0 \\ 0 & 0 & (1 - \beta_3(k)) \frac{v_3 T_s}{l_4} & 1 - \frac{v_4 T_s}{l_4} \end{bmatrix} \begin{bmatrix} \rho_1 \\ \rho_2 \\ \rho_3 \\ \rho_4 \end{bmatrix} (k) \\
 &+ \begin{bmatrix} 0 & \frac{T_s}{l_1} & 0 \\ 0 & 0 & 0 \\ 0 & 0 & 0 \\ 0 & 0 & 0 \end{bmatrix} \begin{bmatrix} q_u \\ r_2 \\ \rho_d \end{bmatrix} (k) + \begin{bmatrix} \frac{w_1 T_s}{l_1} & -\frac{w_2 T_s}{l_1} & 0 & 0 & 0 \\ 0 & \frac{w_2 T_s}{l_2} & 0 & 0 & 0 \\ 0 & 0 & 0 & 0 & 0 \\ 0 & 0 & 0 & 0 & 0 \end{bmatrix} \begin{bmatrix} \rho_{J,1} \\ \rho_{J,2} \\ \rho_{J,3} \\ \rho_{J,4} \\ \rho_{J,5} \end{bmatrix} \\
 &+ \begin{bmatrix} 0 & 0 & 0 & 0 \\ 0 & 0 & -\frac{T_s}{l_2} & 0 \\ 0 & 0 & \frac{T_s}{l_3} & 0 \\ 0 & 0 & 0 & 0 \end{bmatrix} \begin{bmatrix} Q_{M,1} \\ Q_{M,2} \\ Q_{M,3} \\ Q_{M,4} \end{bmatrix} \\
 &= A_3(k)\rho(k) + B_3\mathbf{u}(k) + B_{J,3}(k)\rho_J + B_{Q,3}q_M. \tag{8}
 \end{aligned}$$

The wave front could have occurred between cells 1 and 2, or 3 and 4, instead of 2 and 3; however, the given example serves to illustrate the equation structure for this mode.

In both FC modes, one free-flow-to-congestion transition exists inside the section. Unlike the previous mode, the state matrices change depending on the direction of motion of the wave front. In FC1, the wave front moves downstream. Assuming, for example, that the wave front is between cells 2 and 3, the state equation for this mode is:

$$\begin{aligned}
 \begin{bmatrix} \rho_1 \\ \rho_2 \\ \rho_3 \\ \rho_4 \end{bmatrix} (k+1) &= \begin{bmatrix} 1 - \frac{v_1 T_s}{l_1} & 0 & 0 & 0 \\ \frac{v_1 T_s}{l_2} & 1 - \frac{v_2 T_s}{l_2} & 0 & 0 \\ 0 & \frac{v_2 T_s}{l_3} & 1 & \frac{1}{1 - \beta_3(k)} \frac{w_4 T_s}{l_3} \\ 0 & 0 & 0 & 1 - \frac{w_4 T_s}{l_4} \end{bmatrix} \begin{bmatrix} \rho_1 \\ \rho_2 \\ \rho_3 \\ \rho_4 \end{bmatrix} (k) \\
 &+ \begin{bmatrix} \frac{T_s}{l_1} & 0 & 0 \\ 0 & \frac{T_s}{l_2} & 0 \\ 0 & 0 & 0 \\ 0 & 0 & \frac{w_5 T_s}{l_4} \end{bmatrix} \begin{bmatrix} q_u \\ r_2 \\ \rho_d \end{bmatrix} (k) + \begin{bmatrix} 0 & 0 & 0 & 0 & 0 \\ 0 & 0 & 0 & 0 & 0 \\ 0 & 0 & 0 & -\frac{1}{1 - \beta_3(k)} \frac{w_4 T_s}{l_3} & 0 \\ 0 & 0 & 0 & \frac{w_4 T_s}{l_4} & -\frac{w_5 T_s}{l_4} \end{bmatrix} \begin{bmatrix} \rho_{J,1} \\ \rho_{J,2} \\ \rho_{J,3} \\ \rho_{J,4} \\ \rho_{J,5} \end{bmatrix} \\
 &= A_4(k)\rho(k) + B_4\mathbf{u}(k) + B_{J,4}(k)\rho_J. \tag{9}
 \end{aligned}$$

For FC2, the wave moves upstream. Again assuming that the wave front is between cells 2 and 3, this mode differs from the previous case in that, due to the dominance of the congested flow rate at the wave front boundary, the tri-diagonal row is now the second instead of the third row, and more terms appear in $B_{J,s}$:

$$\begin{aligned}
 \begin{bmatrix} \rho_1 \\ \rho_2 \\ \rho_3 \\ \rho_4 \end{bmatrix} (k+1) &= \begin{bmatrix} 1 - \frac{v_1 T_s}{l_1} & 0 & 0 & 0 \\ \frac{v_1 T_s}{l_2} & 1 & \frac{w_3 T_s}{l_2} & 0 \\ 0 & 0 & 1 - \frac{w_3 T_s}{l_3} & \frac{1}{1-\beta_3(k)} \frac{w_4 T_s}{l_3} \\ 0 & 0 & 0 & 1 - \frac{w_4 T_s}{l_4} \end{bmatrix} \begin{bmatrix} \rho_1 \\ \rho_2 \\ \rho_3 \\ \rho_4 \end{bmatrix} (k) \\
 + \begin{bmatrix} \frac{T_s}{l_1} & 0 & 0 \\ 0 & \frac{T_s}{l_2} & 0 \\ 0 & 0 & 0 \\ 0 & 0 & \frac{w_5 T_s}{l_4} \end{bmatrix} \begin{bmatrix} q_u \\ r_2 \\ \rho_d \end{bmatrix} (k) &+ \begin{bmatrix} 0 & 0 & 0 & 0 & 0 \\ 0 & 0 & -\frac{w_3 T_s}{l_2} & 0 & 0 \\ 0 & 0 & \frac{w_3 T_s}{l_3} & -\frac{1}{1-\beta_3(k)} \frac{w_4 T_s}{l_3} & 0 \\ 0 & 0 & 0 & \frac{w_4 T_s}{l_4} & -\frac{w_5 T_s}{l_4} \end{bmatrix} \begin{bmatrix} \rho_{J,1} \\ \rho_{J,2} \\ \rho_{J,3} \\ \rho_{J,4} \\ \rho_{J,5} \end{bmatrix} \\
 &= A_5(k)\rho(k) + B_5 u(k) + B_{J,5}(k)\rho_J. \tag{10}
 \end{aligned}$$

At each time step, the SMM determines its mode based on the measured mainline boundary data and the congestion status of the cells in the section. If both ρ_u and ρ_d have free-flow status (i.e., both densities are below ρ_c), the FF mode is selected, and if both of these densities are congested (i.e., both densities are at or above ρ_c), the CC mode is selected. If ρ_u and ρ_d are of opposite status, then the SMM performs a search over the ρ_i to determine whether there is a status transition inside the section. This wave front search consists of searching through the cells, in order, looking for the first status transition between adjacent cells (7).

The CTM and SMM were validated on a 2 mile (3km) segment of I-210W, and shown to perform similarly to one another (6, 7), and to have reasonable agreement with observed values. The quality of density estimates can be improved by using output feedback, e.g., in (13, 14) a mixture-Kalman filter (MKF)-based estimator is applied to two of the SMM modes (FF and CC), and at each time step, the estimator determines which of these modes is stochastically most likely, i.e., whether the FF or CC model is a better fit for each freeway section. Through its estimation of the congestion mode, the MKF-based estimator alleviates the need to specify a set of logical mode-selection rules, such as those described in this paper and in (6, 7). The MKF-based estimator has been tested using traffic measurements from I-210W and has been shown to accurately predict traffic densities and congestion modes (13, 14).

Observability and Controllability

The observability and controllability properties of the SMM modes are presented here, since these properties are of fundamental importance for the design of data estimators and ramp-metering control systems. Loosely, controllability answers the question of whether a control input (e.g., a regulated on-ramp flow) can affect the model state (in this case, traffic density). Observability answers the question of whether the measurements taken at a particular detector station (along with knowledge of the system inputs) can be used to reconstruct the initial system state. A more thorough discussion of these properties can be found in (15).

Table 1 summarizes the observability and controllability for each SMM mode. The observability and controllability results were derived using standard linear systems techniques. In the first and second columns, “upstream cells” and “downstream cells” give the status of cells both upstream and downstream of the congestion wave front. If there is no such wave front, both sets of cells have the same status. The third column indicates which of the two mainline boundary measurements, if either, can be used to make the SMM observable. The fourth column states whether the SMM is controllable from an on-ramp at the upstream end of the section, or an on-ramp at the downstream end of the section.

The observability results can be obtained by computing the observability Grammians for the A_s of Eq. (5) with the output matrices $C_u = [I \ 0 \ 0 \ 0]$ and $C_d = [0 \ 0 \ 0 \ I]$, as shown in (7). From the table, it can be seen, as a general result, that if all cells have free-flow status, the densities are observable using a downstream measurement, while in congested mode, they are observable using an upstream measurement. If there is no downstream measurement available when cells are in free-flow mode, or there is no upstream measurement when cells are congested, as in the last two cases listed in Table 1, the system is unobservable. This is related to the wave (information) propagation directions on a freeway in different congestion modes. When a freeway section is in free-flow mode, information propagates downstream at speed v , which is the vehicle traveling speed. Therefore, in order to be able to estimate the cell densities, the downstream density measurement is needed. When the freeway is in congestion, information propagates upstream at speed w , and an upstream measurement is needed to estimate densities.

TABLE 1 Observability and Controllability for Different SMM Modes

Upstream Cells	Downstream Cells	Observable with	Controllable from
Free-flow	Free-flow	Downstream Measurement	Upstream On-Ramp
Congested	Congested	Upstream Measurement	Downstream On-Ramp
Congested	Free-flow	Upstream and Downstream Measurement	Not Controllable
Free-flow	Congested 1	Unobservable	Upstream and Downstream On-Ramp
Free-flow	Congested 2	Unobservable	Upstream and Downstream On-Ramp

The controllability results can be derived in a similar manner as the observability results. Generally, a section in free-flow mode is controllable from an on-ramp at its upstream end, whereas a congested section can be controlled from an on-ramp at its downstream end. If a section is in CF mode, it cannot be controlled by an on-ramp at either end of the section, while the FC modes are controllable from an upstream/downstream on-ramp pair. These controllability results have motivated the design of a traffic-responsive, LQI-based local ramp

metering regulator that switches between using either upstream or downstream densities for feedback, depending on whether the freeway section surrounding the regulated on-ramp has congested or free-flow status. This regulator has been shown to significantly reduce total travel times (compared to the no-metering case), as well as perform favorably compared against regulators such as ALINEA (16) and SWARM (17), in simulation tests using calibrated VISSIM and CTM simulations of I-210W (1, 2).

CELL TRANSMISSION MODEL CALIBRATION METHOD

In this section, a methodology for tuning the CTM and SMM parameters to reproduce observed freeway traffic behavior is described. The calibration method, previously presented in (8), has been tested on a 14-mile (23 km) stretch of I-210W (Figure 1) that typically endures heavy congestion during the weekday morning commute period.

Freeway Representation and Traffic Data

The 14-mile (23 km) I-210W test segment was divided into 41 cells, adapted from a 40-cell partition that was designed by Gabriel Gomes for use in the optimization work of (18, 19). The number of mixed-flow lanes ranges from 4 to 6, with a single high-occupancy vehicle (HOV) lane running parallel to the leftmost mainline lane. The HOV lane is separated from the mainline lanes by a double yellow line, except at six gate locations dispersed throughout the test segment. There are 22 mainline detector stations, each containing one loop-sensor per lane, within the segment. For the 41-cell partition, each cell contains either 0 or 1 detector stations. In the chosen partitioning method, cell boundaries are placed on the mainline immediately upstream of on-ramps and immediately downstream of off-ramps. The minimum, maximum, and mean cell lengths in the partition were 962 ft (293 m), 4012 ft (1224 m), and 1807 ft (551 m). A detailed schematic of the partition can be found in (8).

A CTM simulator was developed in C. Its main inputs include the freeway geometry, model parameters, initial condition, time-series demand profiles at each entrance, and the simulation time step (default is 10 seconds for the 41-cell partition) (8). Most of the traffic data used in the model calibration was obtained from the Performance Measurement System (PeMS) (20), developed by researchers at U.C. Berkeley. Each freeway loop detector provides measurements of volume (veh/timestep) and percent occupancy every 30 seconds, and PeMS aggregates this data from freeways throughout California. In the case of mainline detectors, densities (vpm) are computed for each lane using $density = occupancy / g\text{-factor}$, where the g -factor is the effective vehicle length, in miles, for that detector. For single loop-detector freeways such as I-210, PeMS provides g -factors calculated according to the PeMS algorithm, described in (21). If one or more loops at a mainline station were found to be dead, scaling-corrected aggregates were prepared for use in this study. A scaling correction consists of taking the mean of the densities (or flows) over the functioning loops at a mainline station, then multiplying by the total number of loops. In cases where PeMS on-ramp data was incomplete, demands were reconstructed using a set of manually-counted I-210W ramp flows provided by Caltrans. The reader is referred to (7, 8) for additional details on data processing, demand reconstruction, split ratio estimation, and HOV modeling.

Calibration Methodology

The main steps of the calibration procedure are as follows:

1. **Free-flow Parameter Calibration:** The free-flow traffic velocities, v_i , are determined by performing a least-squares fit on the flow versus density data over the period 5:00–6:00AM. For the I-210 section, traffic typically flows freely during this period. For the j^{th} detector station, v_j is the solution, in the least-squares sense, to the equation $\Phi_j v_j = Y_j$, where Φ_j and Y_j are column vectors that respectively contain densities and flows measured over the specified time interval. The free-flow speed v_j is assigned to the cell containing detector j , and free-flow speeds are computed for cells that do not contain detectors by linear interpolation.
2. **Bottleneck Identification:** Bottleneck locations are identified by examining contour plots of the measured traffic densities and/or speeds, and determining the locations of fixed spatial boundaries which divide the freeway into an upstream congested region and a downstream free-flow region. For example, in the top plot of Fig. 5, a bottleneck was observed to form between the detectors at 33.05 and 32.20 during the 6:00 time slice.
3. **Non-Bottleneck Capacity Selection:** A set of nominal $Q_{M,i}$ are assigned to the cells that are not located at bottlenecks. It is not advisable to set $Q_{M,j}$ equal to the maximum observed flow at each detector-equipped cell, since this will most likely result in underestimating the true capacity of the freeway. Typically, the nominal $Q_{M,i}$ must be chosen to be larger than the maximum observed flows (usually ≥ 2000 vphpl) in each region of the freeway.
4. **Bottleneck Capacity Determination:** Consider a freeway portion divided into two consecutive cells, 1 and 2, where an active bottleneck exists between the two cells; hence, the upstream cell (#1) is congested, while the downstream cell (#2) remains in free-flow status. Further assume that an on-ramp (with merging flow r_2 entering cell 2) enters between the two cells. It can be shown that the bottleneck capacity in this situation is represented by $Q_{M,2} = q_2 + r_2$, where q_2 is the modeled flow entering cell 2 from the mainline (7, 8). Assuming both q_2 and r_2 are measurable, these quantities are used to estimate the bottleneck flow rate, with the default method (assuming no faulty or missing data) being

$$\hat{Q}_{M,2} = \text{mean}_{k \in K_M} (q_2(k) + r_2(k)).$$

K_M corresponds to the half-hour time interval ending at $\arg \max (q_2(k) + r_2(k))$. Determination of the causes and evolution of bottlenecks, and estimation of the ensuing capacities, are active areas of research. For a recent example, see (22).

5. **Congestion Parameter Calibration:** w_i and $\rho_{J,i}$ are estimated by performing a constrained least-squares fit on the flow versus density measurements. First, the critical density is estimated for each detector: $\hat{\rho}_{c,j} = \max_k (q_{dj}(k)) / v_j$, where q_{dj} is the flow measured at detector j . The $(\rho_{dj}(k), q_{dj}(k))$ data is sorted so that only congested pairs are used in the estimation. Let $\kappa = \{k_1 \dots k_{N_c}\}$ denote the set of all k for which $\rho_{dj}(k) > \hat{\rho}_{c,j}$. $[w_j \ w_j \ \rho_{J,j}]^T$ is the solution, in the least squares sense, to $\Phi_j [w_j \ w_j \ \rho_{J,j}]^T = Y_j$, where

$$\Phi_j^T = \begin{bmatrix} -\rho_{dj}(k_1) & \dots & -\rho_{dj}(k_{N_c}) \\ 1 & \dots & 1 \end{bmatrix}, \quad Y_j = \begin{bmatrix} q_{dj}(k_1) + \frac{l_j}{T_s} \Delta \rho_{dj}(k_1) \\ \vdots \\ q_{dj}(k_{N_c}) + \frac{l_j}{T_s} \Delta \rho_{dj}(k_{N_c}) \end{bmatrix},$$

and $\Delta \rho_{dj}(k) = \rho_{dj}(k+1) - \rho_{dj}(k)$, subject to the constraint

$$Q_{M,j} \leq \frac{v_j w_j \rho_{J,j}}{v_j + w_j},$$

which can be written as linear in $[w_j \ w_j \ \rho_{J,j}]^T$. The constraint is included to prevent the solution $[w_j \ w_j \ \rho_{J,j}]^T$ from limiting the maximum possible flow in cell j below the $Q_{M,j}$ determined in previous steps. Note that $\Phi_j [w_j \ w_j \ \rho_{J,j}]^T = Y_j$ is a rewriting of the congested case of the CTM, where $q_{dj}(k)$ is taken as a measurement of the flow exiting the cell containing detector j .

Currently, only values of w_j that fall within a range that is considered physically reasonable, $10 \leq w_j \leq 20$ mph (between 16 and 32 kph), are retained. If the constrained least squares solution does not yield w the acceptable range for a particular detector cell n , this cell is assigned the w_j of the nearest downstream neighbor with a w inside the range. The corresponding $\rho_{J,n}$ is found by solving the equality case of the constraint. w_i and $\rho_{J,i}$ are then determined for non-detector cells through linear interpolation.

6. **Time-Varying Parameter Adjustments:** If necessary, temporary parameter changes (e.g., reduction of $Q_{M,i}$ in a region) can be applied to reproduce the effect of an incident. Also, by reducing w_i in the mid-morning time range, when the traffic is still congested but beginning its recovery back to the free-flow mode, the effect of flow-density hysteresis can be approximated.

Results and Discussion

The calibration methodology was first applied to data from a 2 mi (3 km) subsection of the I-210 testbed, using measurements from 04/25/01. This 4-lane subsection spans three mainline detector stations (at postmiles 34.05, 33.05, and 32.20, from upstream to downstream), and contains 2 on-ramps and 2 off-ramps. The resulting calibrated parameters showed little spatial variation: 60-62 mph (97-100 kph) for v , 2000 vphpl for Q_M , 15 mph (24 kph) for w , and 168-169 vpmpl (104-105 vpkpl) for ρ_J . These parameters were implemented in both the CTM and SMM, and the simulated densities and flows in the middle of the section (near postmile 33.05) were compared with the measured values at that location, as shown in Figure 4. It can be seen that the densities and flows predicted by the models are similar to one another and agree reasonably well with the measured values, although the models tended to overestimate density during the peak congestion hours. These results are very similar to those of the CTM and SMM validation tests of (6, 7), in which hand-tuned parameters were applied to the same freeway section. A more detailed description of the section geometry, cell partition, and data processing methods can be found in (6, 7).

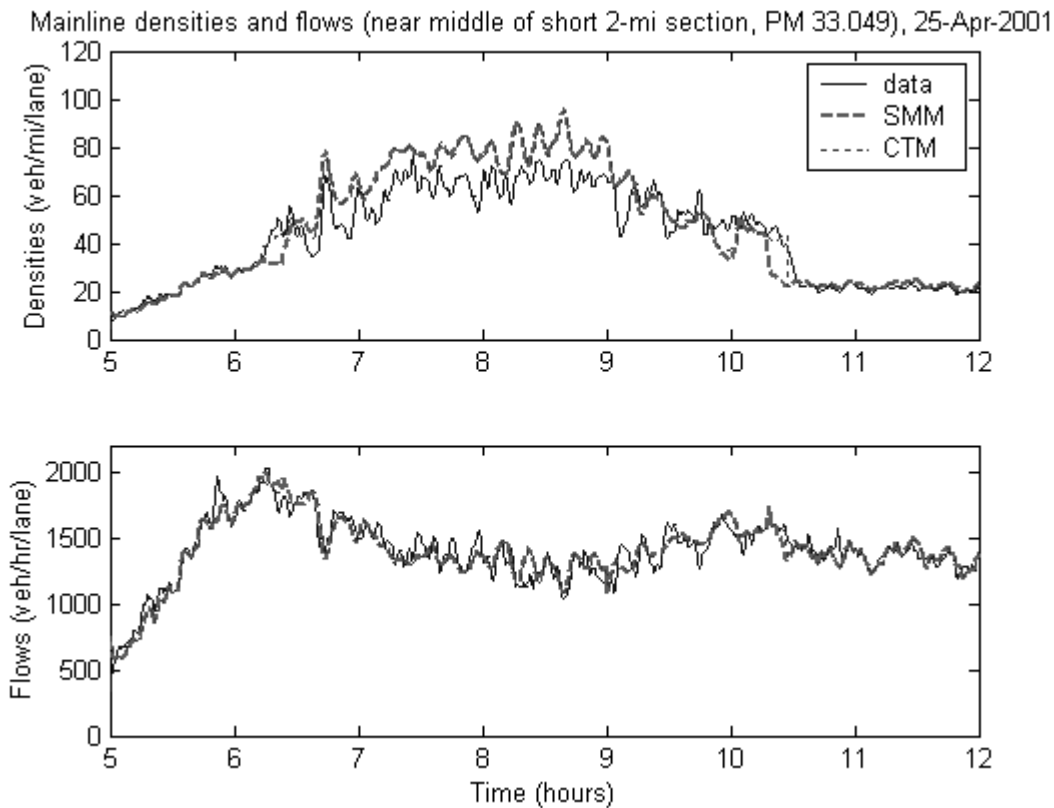


FIGURE 4 Measured and simulated mainline densities and flows, for the detector station at PM 33.05, on April 25, 2001.

The calibration method has also been applied to the full 14-mi section. Fig. 5 shows contour plots for the measured (top) and simulated CTM (bottom) densities for a particular day (Wednesday, Nov. 28, 2001) in the I-210 testbed. The numbers inside the cells are traffic densities (vpmp). Free-flow densities (0–33 vpmp, 0–21 vpkpl) are shown as white. Mid-range congestion (33–43 vpmp, 21–27 vpkpl) is medium gray. Dark gray indicates heavy congestion (43 vpmp (27 vpkpl) or greater). Traffic is flowing from left to right in these plots, and the time, in 15-minute intervals, is given in the leftmost column. The time range is 5:30–10:30AM. Loop detector outages are indicated by crossed-out boxes in the measured-data contour plot. Loop detectors which were suspected to be faulty for the whole day have their postmile labels surrounded by a dashed box at the top of the measured-data plot. If a detector was classified as faulty due to outages in some, but not all, of the lanes, the corresponding “measured” density displayed in the contour plot is a scaling-reconstructed estimate. The simulation time step size used for the model was 10 seconds.

The nominal $Q_{M,i}$ was chosen as 2300 vphpl for the 5 cells farthest upstream, and 2100 vphpl for the remaining cells. Visual assessment of the density contour plots yielded suspected bottlenecks at postmiles 33.05, 30.78, 29.88, 28.03, and 26.12. Two additional days (Tuesday,

1
2
3
4 Nov. 13, 2001, and Thursday, Jan. 10, 2002) were tested, and relative to Jan. 10, 2002, these
5 days had more faulty data in the middle region of the freeway. Reconstructive methods were
6 used to estimate $Q_{M,i}$ at several bottlenecks. Specifically, missing flow data was compensated
7 depending on the availability of nearby measurements, resulting in a flow balance equation, a
8 historical average, and a local scaling reconstruction, at postmiles 30.78, 28.88, and 28.03,
9 respectively (7). An area of ongoing work is to determine an improved procedure for estimating
10 bottleneck capacities in cases where the nearby mainline flow data is incomplete. Non-
11 reconstructed data were used wherever possible in the calibration tests; in particular, faulty
12 mainline detector stations were left out of the estimation of v_i , w_i , and $\rho_{J,i}$, which were then
13 interpolated, using the methods described previously, from the nearest available values. Use of
14 reconstructed values was unavoidable in the estimation of $Q_{M,i}$ at certain bottlenecks, though,
15 since bottlenecks require estimation of flow conditions in their immediate vicinity. The
16 calibrated parameters showed spatial variation on each test day, and the resulting ranges were:
17 58-68 mph (94-109 kph) for v , 1488-2300 vphpl for Q_M , 14-19 mph (22-31 kph) for w , and 143-
18 188 vpmpl (89-117 vpkpl) for ρ_J . A more detailed analysis of the parameters can be found in (7).
19
20
21
22
23
24
25
26
27
28
29
30
31
32
33
34
35
36
37
38
39
40
41
42
43
44
45
46
47
48
49
50
51
52

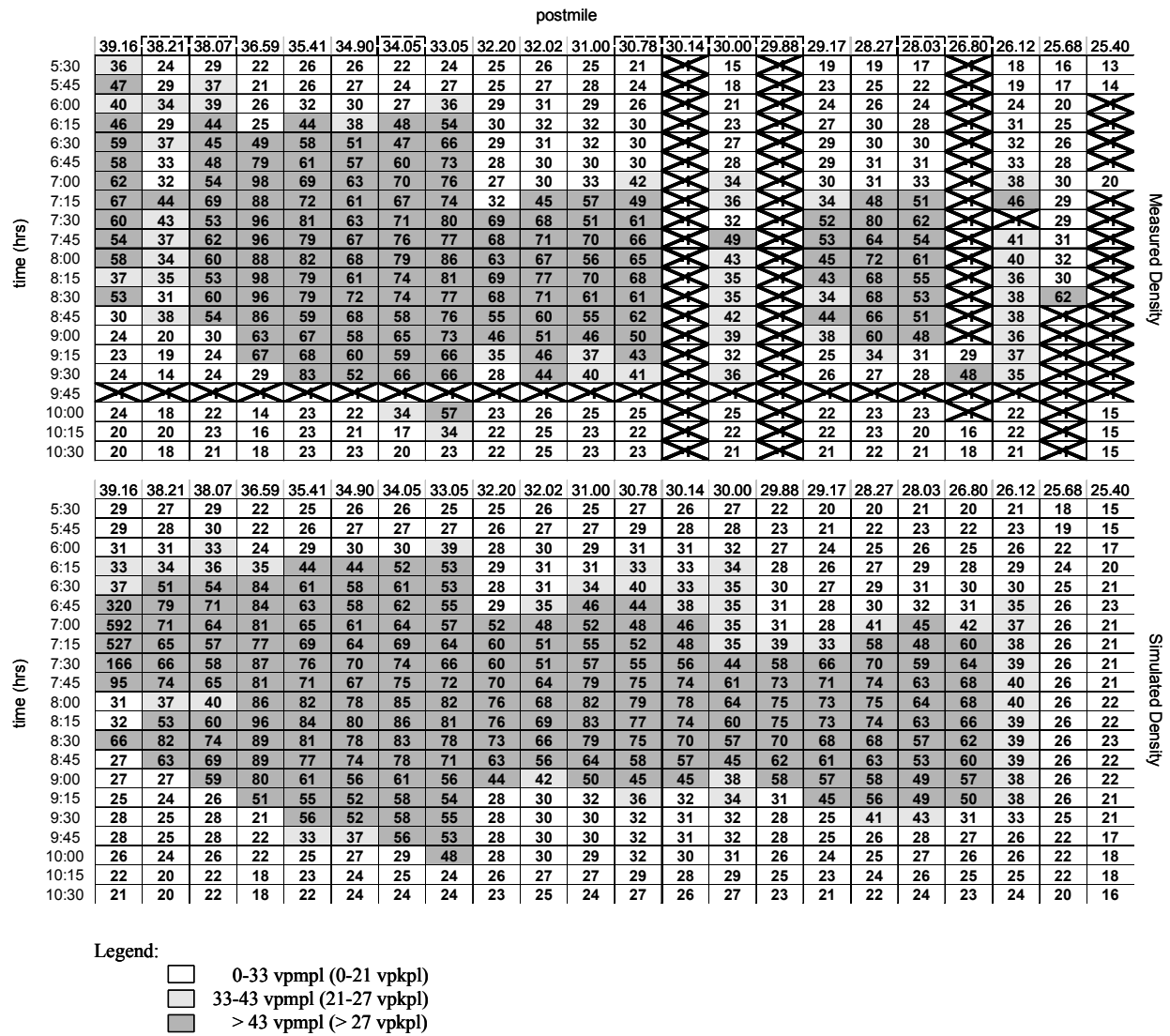


FIGURE 5 Contour plots of 15-minute average measured densities (top) and simulated CTM densities (bottom), vpmp, for Nov. 28, 2001. (1 vpmp = 0.62 vpkpl)

To evaluate the performance of the simulation, we define a partial Total Travel Time:

$$TTT = T_s \sum_{k=k_5:00}^{k_{11:45}} \sum_{i \in C_d} l_i \rho_i(k).$$

Here, C_d is the set of cells which had problem-free mainline detectors over each of the examined days. C_d excludes detectors at postmiles 38.21, 38.07, 34.05, 30.78, 30.14, 30.00, 29.88, 28.03, 26.80, and 25.40. Although it functions properly, the detector at 39.16 is also excluded, since the CTM boundary condition prevents the model from accurately reproducing congestion that (in the real system) spills upstream outside of the simulated region. Results for TTT are summarized in Table 2, along with the spatial mean of the mean percentage error (MMPE) at the non-excluded detectors, defined as

$$E_{MMPE} = 100 \times \frac{1}{N_{C_d}} \sum_{i \in C_d} \frac{1}{M} \sum_{k=1}^M \left| \frac{\rho_i(k) - \hat{\rho}_i(k)}{\rho_i(k)} \right|,$$

where N_{C_d} is the number of non-excluded detectors (11 out of 22 in this case).

TABLE 2 Total Travel Time (veh-hr) and mean MPE for three different days

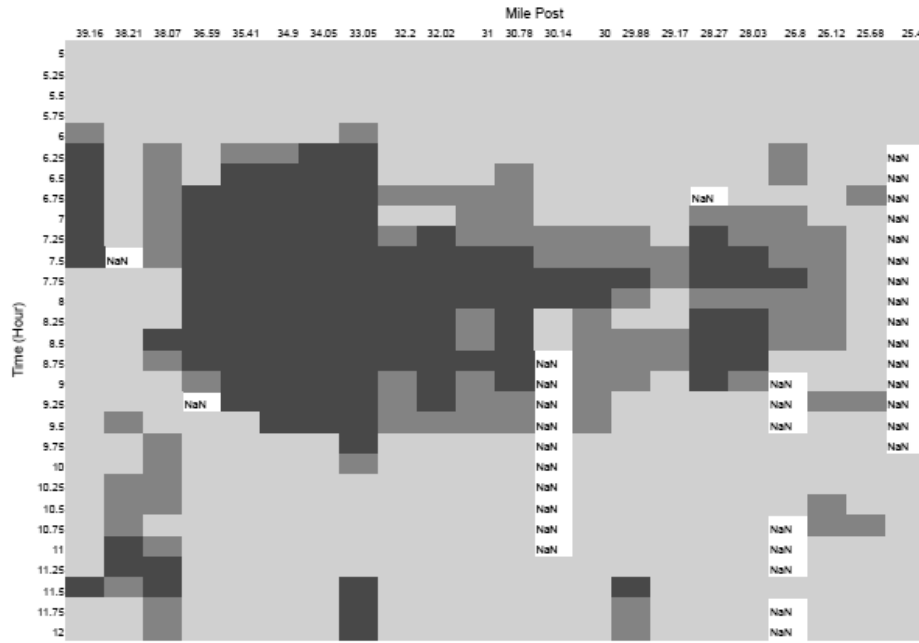
Date	Meas.	Sim.	% TTT Err.	MMPE
Jan. 10, 2002	3778	3766	-0.32	14.2
Nov. 28, 2001	4273	4278	0.01	14.2
Nov. 13, 2001	4163	3961	-4.85	16.1
mean	4071	4002	-1.72	14.8
std. dev.	260	258	2.71	1.1

The values of MMPE are not surprising, since they are similar to the MPEs in the short-segment validation tests of (6). From Figure 5 and Table 2, it can be seen that the CTM reproduces the observed bottlenecks and the approximate duration and spatial extent of the congestion upstream of each bottleneck, and predicts the total travel time with approximately 2% mean error over three days. The top plot of Fig. 5 shows that the backward-traveling shock wave emanating from the bottleneck near postmile 33.05 after 6AM travels faster than the forward-traveling shock (dissipation wave) that reaches the same bottleneck after 10AM. These features, which are observed in the data, are reproduced by the model. Simulation tests documented in (7) indicate that TTT is more sensitive to Q_M than other model parameters.

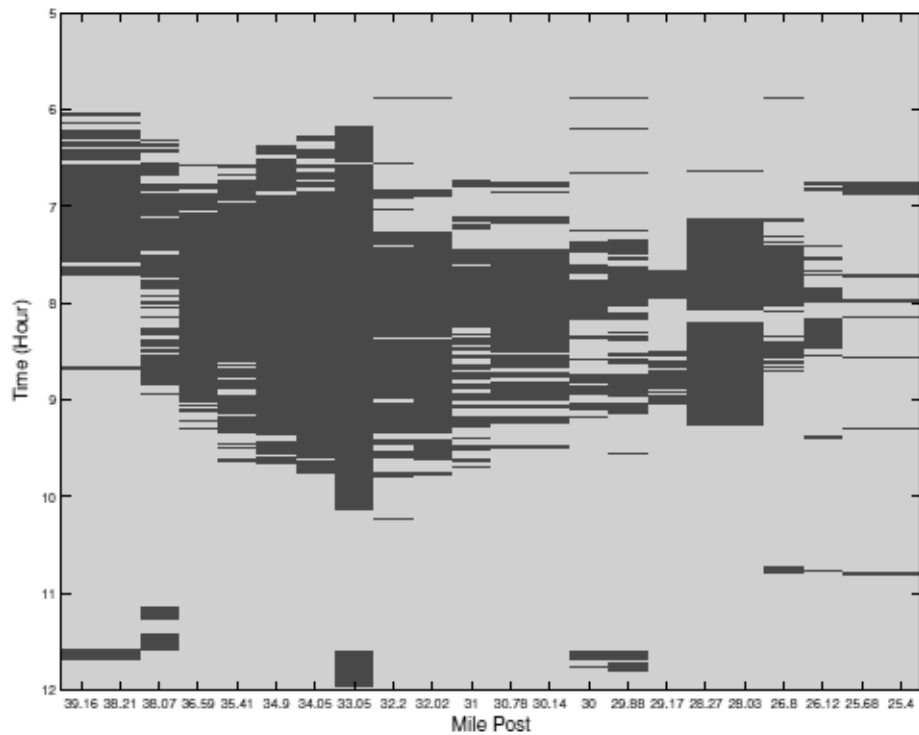
The automated steps of the calibration method have been determined to have a low computational cost. The most time-consuming automated step of the calibration process is the constrained linear least squares estimation of congestion parameters for each cell, which can be carried out for the 14-mile (23 km) portion of I-210W, partitioned into 41 cells, in less than 1 minute for 7 hours of 5-minute average measurement data on a 1.0 GHz, 256 MB Pentium III computer. The computer simulation speed of the CTM itself is high: a simulation of the 14-mile portion of I-210W, for the same partition and time range, with a 10-second model time step, can be completed in less than 10 seconds on the aforementioned computer.

1
2
3
4 The single-wave front assumption of the SMM, discussed previously, means that the
5 SMM is expected to be suitable for short freeway sections; the model requires modification to
6 handle longer sections, which are more likely to contain multiple wave fronts simultaneously.
7 However, this issue can be avoided in the design of a closed-loop estimator. In this case, a long
8 segment can be broken into a series of shorter segments (the typical distance between
9 functioning I-210 mainline stations is appropriate), and a series of SMMs can be put together to
10 produce state estimates at unmonitored locations, using feedback from any non-faulty mainline
11 stations that are available at short-segment boundaries. To help illustrate the SMM's usefulness
12 in closed-loop estimation of densities and congestion modes for longer freeway segments, results
13 from (14) are summarized here. A mixture Kalman filtering (MKF) algorithm (23) has been
14 applied to the SMM, and the resulting closed-loop estimator is able to provide estimated vehicle
15 densities at unmeasured locations, as well as the estimated congestion status (free-flow or
16 congested) of each freeway subsection. The program runs efficiently, which makes it possible to
17 carry out estimation in real time (14).

18 This MKF estimator has been tested on the entire 14-mi test segment. Fig. 6(b) shows the
19 congestion mode estimates produced by the estimator, using data from January 10, 2002. In the
20 plot, light gray indicates free-flow mode, and dark gray indicates congested mode. A contour
21 plot of the PeMS-derived 15-minute average speeds for that day is displayed in Fig. 6(a). In this
22 plot, light gray approximately indicates free-flow conditions (an average speed of 55 mph (89
23 kph) and above), and dark gray indicates an average speed of 40 mph (60 kph) and below, in
24 which the traffic is considered to be in congestion. Medium gray corresponds to an average
25 speed between 40 and 55 mph, in which the traffic is somewhat likely to be in congestion. White
26 areas in the plot signify unavailable data. It can be seen from the plots that in general, the MKF-
27 based congestion mode estimates agree with the speed contour plot. Interested readers should
28 refer to (14) for more information.
29
30
31
32
33
34
35
36
37
38
39
40
41
42
43
44
45
46
47
48
49
50
51
52



(a) PeMS 15-minute average speed contour plot (dark gray: <40 mph (64 kph); medium gray: 40–55 mph (64-89 kph); light gray: >55 mph (89 kph)).



(b) MKF congestion-mode estimates (dark gray: congestion; light gray: free-flow).

FIGURE 6 Congestion mode estimation for the 14-mi (23 km) I-210W test segment (January 10, 2002).

Comparison to a Different Method

An imputation algorithm (9) has been developed by Chen et al. to impute bad or missing loop data, using linear regression techniques that incorporate historical values and data from neighboring loops. A data imputation hierarchy that includes a similar algorithm had been implemented in PeMS at the time of this writing; however, imputed data were not used in any of the CTM or SMM studies described previously. In (9), the method was tested on PeMS data from a particular day (4/24/2002), and error measures were computed as averages over 189 loops on California freeways. Two of the reported measures were the mean absolute error (MAE) and mean (M) values for occupancy and flow. For a measured quantity $x(k)$ and its estimate $\hat{x}(k)$, a normalized error measure can be defined by dividing MAE by M:

$$\text{MAE} = \frac{1}{N} \sum_{k=1}^N |x(k) - \hat{x}(k)|, \quad \text{MAE/M} = \frac{\frac{1}{N} \sum_{k=1}^N |x(k) - \hat{x}(k)|}{\frac{1}{N} \sum_{k=1}^N x(k)}.$$

For the CTM results stated previously, averaging MAE/M over the detectors in set C_d , then averaging over all three test days yields 17% and 7%, for density and flow, respectively. MAE/M for the results of (9) are 15% and 11% for occupancy and flow, respectively. It is acknowledged that occupancy and density are not directly comparable, and that normalized test conditions would be required to make a fair comparison between methods. However, these preliminary results suggest that CT-based models can yield flow and density prediction quality that is comparable to a reported method. Hence, these models warrant further investigation as a basis for traffic estimators and controllers.

CONCLUSIONS

In this paper, a macroscopic freeway traffic model, the Switching-Mode Model (SMM), was presented. This model is a piecewise-linearized version of Daganzo's CTM (4, 5), which was found to be computationally efficient and well-suited for implementation in real-time control, estimation, and traffic monitoring applications. The observability and controllability properties of the individual modes of the SMM were stated, since they are of fundamental importance in the design of data estimators and ramp-metering control systems. It was explained that the free-flow traffic mode is observable from a downstream measurement and controllable from an upstream on-ramp, and that the congested mode is observable from an upstream measurement and controllable from a downstream on-ramp.

The following points summarize the main disadvantages and advantages of the CTM relative to the SMM, and vice versa.

CTM:

- Disadvantages: It is a nonlinear model; hence the model-analysis methods and estimator/controller designs will be more complex, and thus potentially slower-performing in real-time applications, than those for a linear model.
- Advantages: The congestion status of a cell (free-flow or congested) can be determined automatically by comparing $\rho_i(k)$ to $\rho_{c,i}$. In addition, unlike the SMM, the model lacks a single-wavefront-per-section assumption.

SMM:

- Disadvantages: Congestion-mode selection rules, such as those described previously, must be supplied to the model. In addition, there is the single wavefront-per-section assumption, also discussed previously.
- Advantages: It yields similar performance (in terms of accuracy and computation time) as the CTM, but with the advantage of possessing a linear mode structure. Linear analysis methods and controller/estimator design techniques can be applied to the individual modes.

Both of the aforementioned disadvantages of the SMM can be mitigated using the closed-loop estimation approach described in (13, 14). The SMM has been found to be well-suited for use in a closed-loop estimator, using feedback from available measurements to estimate densities at unmonitored locations.

A procedure for calibrating the CTM and SMM parameters was summarized. Parameters were first calibrated for a short (2 mi (3 km)) subsection of I-210W and tested on both the SMM and CTM, which were shown to perform similarly to one another, and to have reasonable agreement with observed values. A calibrated CTM model was tested on the full 14-mile (23 km) test section of I-210W, and has been shown to reproduce the main features of the observed traffic congestion on the freeway, such as approximate location of bottlenecks and duration and spatial extent of congestion. In addition, the model accurately predicts the total travel time (TTT) in the freeway. A main benefit of the overall calibration method is that it provides a well-defined, partially automated procedure for using loop detector data to estimate free-flow speeds, congestion parameters, and bottleneck capacities for these models.

ACKNOWLEDGEMENTS

This research was supported by Partners for Advanced Transit and Highways (PATH) Task Orders 4136 and 5503.

REFERENCES

- (1) Sun, X. and R. Horowitz. A Localized Switching Ramp-Metering Controller with a Queue Length Regulator for Congested Freeways. In *Proceedings of the 2005 American Control Conference*, Portland, Oregon, USA, June 8–10, 2005, pp. 2141-2146.
- (2) Sun, X. and R. Horowitz. Localized Switching Ramp-Metering Control with Queue Length Estimation and Regulation and Microscopic Simulation Results. In *Proceedings of the 16th IFAC World Congress*, Prague, Czech Republic, 2005.
- (3) Zhang, L., J. Colyar, J. Halkias, and Y. Zhang. CORSIM Sensitivity Analysis and its Application in Model Validation and Calibration at Signalized Intersections. In *Transportation Research Board 83rd Annual Meeting*. CD-ROM. Washington, D.C., USA, January 2004.

- (4) Daganzo, C. F. The Cell Transmission Model: A Dynamic Representation of Highway Traffic Consistent with the Hydrodynamic Theory. *Transportation Research - B*, Vol. 28, No. 4, 1994, pp. 269-287.
- (5) Daganzo, C. F. The Cell Transmission Model, Part II: Network Traffic. *Transportation Research - B*, Vol. 29, No. 2, 1995, pp. 79-93.
- (6) Muñoz, L., X. Sun, R. Horowitz, and L. Alvarez. Traffic Density Estimation with the Cell Transmission Model. In *Proceedings of the 2003 American Control Conference*, Denver, Colorado, USA, June 2003, pp. 3750-3755.
- (7) Muñoz, L. *Macroscopic Modeling and Identification of Freeway Traffic Flow*. Ph.D. Dissertation, University of California, Berkeley, 2004.
- (8) Muñoz, L., X. Sun, D. Sun, G. Gomes, and R. Horowitz. Methodological Calibration of the Cell Transmission Model. In *Proceedings of the 2004 American Control Conference*, Boston, Massachusetts, USA, June 30 – July 2, 2004, pp. 798-803.
- (9) Chen, C., J. Kwon, A. Skabardonis, and P. Varaiya. Detecting Errors and Imputing Missing Data for Single Loop Surveillance Systems. In *Transportation Research Board 82nd Annual Meeting*, Washington, D.C., USA, January 2003.
- (10) Lin, W.-H., and D. Ahanotu. *Validating the Basic Cell Transmission Model on a Single Freeway Link*. PATH Technical Note 95-3. Institute of Transportation Studies, University of California, Berkeley, 1994.
- (11) Daganzo, C. F. A Finite Difference Approximation of the Kinematic Wave Model of Traffic Flow. *Transportation Research - B*, Vol. 29, No. 4, 1995, pp. 261-276.
- (12) Gomes, G., A. May, and R. Horowitz. Calibration of Vissim for a Congested Freeway. PATH Research Report UCB-ITS-PRR-2004-4, Institute of Transportation Studies, University of California at Berkeley, 2004.
- (13) Sun, X., L. Muñoz, and R. Horowitz. Highway Traffic State Estimation Using Improved Mixture Kalman Filters for Effective Ramp Metering Control. In *Proceedings of the 42nd IEEE Conference on Decision and Control*, Maui, Hawaii, USA, Dec. 9–12, 2003, pp. 6333-6338.
- (14) Sun, X., L. Muñoz, and R. Horowitz. Mixture Kalman Filter Based Highway Congestion Mode and Vehicle Density Estimator and its Application. In *Proceedings of the 2004 American Control Conference*, Boston, Massachusetts, USA, June 30 – July 2, 2004, pp. 2098-2103.
- (15) Brogan, W.L. *Modern Control Theory*. Prentice Hall, 3rd edition, 1991.
- (16) Papageorgiou, M., H. Hadj-Salem, and J.M. Blosseville. ALINEA: A Local Feedback Control Law for On-ramp Metering. In *Transportation Research Record: Journal of the*

1
2
3
4
5
6
7
8
9
10
11
12
13
14
15
16
17
18
19
20
21
22
23
24
25
26
27
28
29
30
31
32
33
34
35
36
37
38
39
40
41
42
43
44
45
46
47
48
49
50
51
52

Transportation Research Board, No. 1320, TRB, National Research Council, Washington, D.C., 1991, pp. 58-64.

(17) *System Wide Adaptive Ramp Metering High Level Design*. Technical report, National Engineering Technology Corporation, 14320 Firestone Boulevard, Suite 100, La Mirada, CA 90638. June, 1996.

(18) Gomes, G. and R. Horowitz. Globally Optimal Solutions to the Onramp Metering Problem, part I. In *Proceedings of the 7th International IEEE Conference on Intelligent Transportation Systems*, Washington, D.C., USA, 2004, pp. 509-514.

(19) Gomes, G. and R. Horowitz. Globally Optimal Solutions to the Onramp Metering Problem, part II. In *Proceedings of the 7th International IEEE Conference on Intelligent Transportation Systems*, Washington, D.C., USA, 2004, pp. 515-520.

(20) Freeway Performance Measurement System (PeMS). The PeMS Group.
<http://pems.eecs.berkeley.edu/>. Accessed October 2002.

(21) Jia, Z., C. Chen, B. Coifman, and P. Varaiya. The PeMS Algorithms for Accurate, Real-Time Estimates of g-factors and Speeds from Single-Loop Detectors. In 2001 IEEE Intelligent Transportation Systems Conference Proceedings, Oakland, CA, USA, August 2001, pp. 536-541.

(22) Bertini, R. L. and M. J. Cassidy. Some observed queue discharge features at a freeway bottleneck downstream of a merge. *Transportation Research – A*, Vol. 36, 2002, pp. 683-697.

(23) Chen, R., and J. S. Liu. Mixture Kalman filters. *Journal of the Royal Statistical Society, Series B – Statistical Methodology*, vol. 62, 2000, pp. 493–508.